

Windowed Green Function method for the Helmholtz equation in presence of multiply layered media

Oscar P. Bruno*¹ and Carlos Pérez-Arancibia²

¹Computing & Mathematical Sciences, California Institute of Technology.

²Department of Mathematics, Massachusetts Institute of Technology.

December 17, 2021

Abstract

This paper presents a new methodology for the solution of problems of two- and three-dimensional acoustic scattering (and, in particular, two-dimensional electromagnetic scattering) by obstacles and defects in presence an arbitrary number of penetrable layers. Relying on use of certain slow-rise windowing functions, the proposed Windowed Green Function approach (WGF) efficiently evaluates oscillatory integrals over unbounded domains, with high accuracy, without recourse to the highly expensive Sommerfeld integrals that have typically been used to account for the effect of underlying planar multi-layer structures. The proposed methodology, whose theoretical basis was presented in the recent contribution (SIAM J. Appl. Math. 76(5), p. 1871, 2016), is fast, accurate, flexible, and easy to implement. Our numerical experiments demonstrate that the numerical errors resulting from the proposed approach decrease faster than any negative power of the window size. In a number of examples considered in this paper the proposed method is up to thousands of times faster, for a given accuracy, than corresponding methods based on use of Sommerfeld integrals.

1 Introduction

This paper presents a new methodology for the solution of problems of acoustic scattering by obstacles and defects in presence an arbitrary number of penetrable layers in two and three-dimensional space; naturally, the two-dimensional Helmholtz solvers also apply, by mathematical analogy, to corresponding two-dimensional electromagnetic scattering problems. This “Windowed Green Function” (WGF) method, whose theoretical basis was presented in the recent contribution [4], is based on use of smooth windowing functions and integral kernels that can be expressed directly in terms of the free-space Green function, and, importantly, it *does not require use of expensive Sommerfeld integrals*. The proposed methodology is fast, accurate, flexible, and easy to implement. Our experiments demonstrate that, as predicted by theory, the numerical errors resulting from the proposed approach decrease faster than any negative power of the window size. In a number of examples considered in this paper the proposed method is up to thousands of times faster, for a given accuracy, than corresponding methods based on use of Sommerfeld integrals.

*obruno@caltech.edu

The classical layer Green functions and associated Sommerfeld integrals automatically enforce the relevant transmission conditions on the unbounded flat surfaces and thus reduce the scattering problems to integral equations on the obstacles and/or defects (cf. [19, 24]). The Sommerfeld integrals amount to singular Fourier integrals [8, 25] whose evaluation is generally quite challenging. A wide range of approaches have been proposed for evaluation of these quantities [1, 6, 7, 12, 13, 18, 21, 22, 23] but, as is known, all of these methods entail significant computational costs [6, 18, 19, 21].

The WGF approach proceeds as follows. The integral equation formulations of the scattering problems under consideration, which are at first posed on the complete set of material interfaces (including all unbounded interfaces), are then *smoothly truncated* to produce an approximating integral-equation system posed over bounded integration domains that include the surface defects and relatively small portions of the flat interfaces. The integral-operator truncation is effected by means of a certain *slow-rise smooth window function* which, importantly, gives rise to solution errors which decrease faster than any negative power of the window size. In practice the proposed solution method is up to thousands of times faster, for a given accuracy, than corresponding methods [23] based on use of Sommerfeld integrals; the speedups in evaluations of near fields are even more significant, in view of the large computing times required for evaluation of Sommerfeld integrals near the planar interface.

This paper is organized as follows. Section 2 presents a description of the multilayer scattering problem. Section 3 then presents two types of direct multi-layer integral equations for a physical, which can be obtained by means of a generalized version of Green’s third identity (which is itself derived in Appendix A). The windowed integral equations are derived in Section 4 and the corresponding expressions for the field evaluation are presented in Section 5. Section 7, finally, presents a variety of numerical examples which demonstrate the super-algebraic convergence and the efficiency of the proposed approach.

2 Preliminaries

We consider the problem of scattering of an acoustic incoming wave by a two- or three-dimensional configuration such as the one depicted in Figure 1b—in which an incoming wave is scattered by localized (bounded) surface defects and/or scattering objects in presence of a layered medium containing a number $N > 1$ of layers. For notational simplicity our descriptions are presented in the two-dimensional case, but applications to three-dimensional configurations are presented in Section 7. The unperturbed configuration, which is shown in Figure 1a for reference, consists of N planar layers given by $D_j = \mathbb{R} \times (-d_j, -d_{j-1})$ for $j = 1, \dots, N$. The planar boundary at the interface between the layers D_j and D_{j+1} is denoted by $P_j = \mathbb{R} \times \{-d_j\}$ ($j = 1, \dots, N - 1$). The corresponding perturbed layers and their boundaries will be denoted by Ω_j , $j = 1, \dots, N$ and Γ_j , $j = 1, \dots, N - 1$, respectively; naturally, it is assumed that $\Gamma_j \cap \Gamma_i = \emptyset$.

Letting $\omega > 0$ and $c_j > 0$ denote the angular frequency and the speed of sound in the layer Ω_j , the wavenumber k_j in that layer is given by $k_j = \omega/c_j$. Assuming e.g. an incident plane wave of the form $u^{\text{inc}}(\mathbf{r}) = e^{ik_1(x \cos \alpha + y \sin \alpha)}$ (where $\mathbf{r} = (x, y)$ and where $-\pi < \alpha < 0$ denotes the angle of incidence measured with respect to the horizontal) and letting u denote the acoustic pressure, the restrictions $u_j = u|_{\Omega_j}$ of the total field u to the domains Ω_j ($j = 1, \dots, N$) satisfy the homogeneous Helmholtz equation

$$\Delta u_j + k_j^2 u_j = 0 \quad \text{in} \quad \Omega_j, \quad j = 1, \dots, N, \quad (1)$$

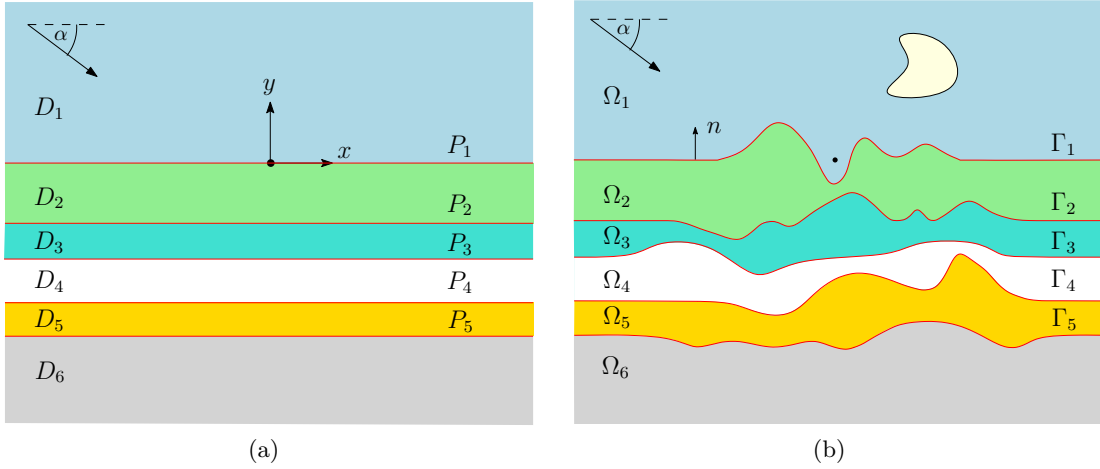


Figure 1: Geometry description of a two- or three-dimensional planar layered medium (a) and a locally perturbed planar layered medium (b) for the case $N = 6$.

together with the transmission conditions

$$u_j = u_{j+1} \quad \text{and} \quad \frac{\partial u_j}{\partial n} = \nu_j \frac{\partial u_{j+1}}{\partial n} \quad \text{on} \quad \Gamma_j, \quad j = 1, \dots, N-1, \quad (2)$$

where $\nu_j = \varrho_j / \varrho_{j+1}$ where ϱ_j denotes the fluid density in Ω_j . For definiteness, here and throughout this paper the unit normal $n = n(\mathbf{r})$ for $\mathbf{r} \in \Gamma_j$ is assumed to point into Ω_j .

As is well known, a closed form expression exists [8, 26] for the total field u^p throughout space ($u^p = u_j^p$ in D_j , $j = 1, \dots, N$), that results as a plane wave u^{inc} impinges on the planar layer medium $D = \cup_{j=1}^N D_j$. In detail, letting $k_{1x} = k_1 \cos \alpha$ and $k_{jy} = \sqrt{k_j^2 - k_{1x}^2}$, $j = 1, \dots, N$ (where the complex square-root is defined in such a way that $\text{Im} k_{jy} \geq 0$, which, noting that $\text{Im} k_j^2 \geq 0$, requires $\text{Re} k_{jy} \geq 0$ as well), the planar-medium solution u_j^p in D_j is given by

$$u_j^p(x, y) = A_j e^{ik_{1x}x} \left\{ e^{-ik_{jy}y} + \tilde{R}_{j,j+1} e^{ik_{jy}(y+2d_j)} \right\} \quad \text{in} \quad D_j, \quad 1 \leq j \leq N, \quad (3)$$

in terms of certain generalized reflection coefficients $\tilde{R}_{j,j+1}$ and amplitudes A_j . The amplitudes and the generalized reflection coefficients can be obtained recursively by means of the relations

$$A_j = \begin{cases} 1 & \text{if } j = 1, \\ \frac{T_{j-1,j} A_{j-1} e^{i(k_{j-1,y} - k_{jy})d_{j-1}}}{1 - R_{j,j-1} \tilde{R}_{j,j+1} e^{2ik_{jy}(d_j - d_{j-1})}} & \text{if } j = 2, \dots, N, \end{cases} \quad (4)$$

and

$$\tilde{R}_{j,j+1} = \begin{cases} 0 & \text{if } j = N, \\ R_{j,j+1} + \frac{T_{j+1,j} \tilde{R}_{j+1,j+2} T_{j,j+1} e^{2ik_{j+1,y}(d_{j+1} - d_j)}}{1 - R_{j+1,j} \tilde{R}_{j+1,j+2} e^{2ik_{j+1,y}(d_{j+1} - d_j)}} & \text{if } j = N-1, \dots, 1, \end{cases} \quad (5)$$

in terms of the reflection and transmission coefficients

$$R_{j,j+1} = \frac{k_{jy} - \nu_j k_{j+1,y}}{k_{jy} + \nu_j k_{j+1,y}} \quad \text{and} \quad T_{j,j+1} = \frac{2k_{jy}}{k_{jy} + \nu_j k_{j+1,y}},$$

respectively.

3 Integral equation formulations

This section presents an integral equation for the unknown interface values of the total field and its normal derivative from below, at each one of the interfaces Γ_j , $j = 1, \dots, N - 1$. As in the contribution [4] we utilize the single- and double-layer potentials

$$\begin{aligned} S_j^t[\phi](\mathbf{r}) &= \int_{\Gamma_{j-1}} G_{k_j}(\mathbf{r}, \mathbf{r}') \phi(\mathbf{r}') \, ds_{\mathbf{r}'}, & D_j^t[\phi](\mathbf{r}) &= \int_{\Gamma_{j-1}} \frac{\partial G_{k_j}}{\partial n_{\mathbf{r}'}}(\mathbf{r}, \mathbf{r}') \phi(\mathbf{r}') \, ds_{\mathbf{r}'}, \\ S_j^b[\phi](\mathbf{r}) &= \int_{\Gamma_j} G_{k_j}(\mathbf{r}, \mathbf{r}') \phi(\mathbf{r}') \, ds_{\mathbf{r}'}, & D_j^b[\phi](\mathbf{r}) &= \int_{\Gamma_j} \frac{\partial G_{k_j}}{\partial n_{\mathbf{r}'}}(\mathbf{r}, \mathbf{r}') \phi(\mathbf{r}') \, ds_{\mathbf{r}'}, \end{aligned} \quad (6)$$

which are defined for $\mathbf{r} \in \mathbb{R}^2$ and are expressed in terms of improper integrals whose convergence is conditioned upon the oscillatory behavior of the integrand. Here we have called $G_{k_j}(\mathbf{r}, \mathbf{r}') = \frac{i}{4} H_0^{(1)}(k_j |\mathbf{r} - \mathbf{r}'|)$ the free-space Green function for the Helmholtz equation with wavenumber k_j . Additionally, we define the integral operators

$$\begin{aligned} K_j^t[\phi](\mathbf{r}) &= \int_{\Gamma_{j-1}} \frac{\partial G_{k_j}}{\partial n_{\mathbf{r}}}(\mathbf{r}, \mathbf{r}') \phi(\mathbf{r}') \, ds_{\mathbf{r}'}, & N_j^t[\phi](\mathbf{r}) &= \int_{\Gamma_{j-1}} \frac{\partial^2 G_{k_j}}{\partial n_{\mathbf{r}} \partial n_{\mathbf{r}'}}(\mathbf{r}, \mathbf{r}') \phi(\mathbf{r}') \, ds_{\mathbf{r}'}, \\ K_j^b[\phi](\mathbf{r}) &= \int_{\Gamma_j} \frac{\partial G_{k_j}}{\partial n_{\mathbf{r}}}(\mathbf{r}, \mathbf{r}') \phi(\mathbf{r}') \, ds_{\mathbf{r}'}, & N_j^b[\phi](\mathbf{r}) &= \int_{\Gamma_j} \frac{\partial^2 G_{k_j}}{\partial n_{\mathbf{r}} \partial n_{\mathbf{r}'}}(\mathbf{r}, \mathbf{r}') \phi(\mathbf{r}') \, ds_{\mathbf{r}'}, \end{aligned} \quad (7)$$

where the evaluation point \mathbf{r} belongs to either Γ_j or Γ_{j-1} .

In order to formulate an integral equation for the unknown interface values we define the unknown density functions $\varphi_j : \Gamma_j \rightarrow \mathbb{C}$ and $\psi_j : \Gamma_j \rightarrow \mathbb{C}$ ($j = 1, \dots, N - 1$) by

$$\varphi_j = u_{j+1} \quad \text{and} \quad \psi_j = \frac{\partial u_{j+1}}{\partial n} \quad \text{on} \quad \Gamma_j. \quad (8)$$

Additionally we define the vector density functions

$$\boldsymbol{\phi}_j = [\varphi_j, \psi_j]^T, \quad \boldsymbol{\phi}^{\text{inc}} = \left[u^{\text{inc}}|_{\Gamma_1}, \frac{\partial u^{\text{inc}}}{\partial n}|_{\Gamma_1} \right]^T \quad \text{and} \quad \boldsymbol{\phi}^{\parallel} = \left[u_N^{\parallel}|_{\Gamma_{N-1}}, \frac{\partial u_N^{\parallel}}{\partial n}|_{\Gamma_{N-1}} \right]^T \quad (9)$$

where u_N^{\parallel} is defined in (52), and the matrix operators

$$\begin{aligned} \mathbf{E}_j &= \begin{bmatrix} 1 & 0 \\ 0 & \frac{1+\nu_j}{2} \end{bmatrix}, \quad \mathbf{T}_j = \begin{bmatrix} D_{j+1}^t - D_j^b & -S_{j+1}^t + \nu_j S_j^b \\ N_{j+1}^t - N_j^b & -K_{j+1}^t + \nu_j K_j^b \end{bmatrix}, \quad \mathbf{L}_j = \begin{bmatrix} D_j^t & -S_j^t \\ N_j^t & -K_j^t \end{bmatrix} \\ \text{and } \mathbf{R}_j &= \begin{bmatrix} -D_{j+1}^b & \nu_{j+1} S_{j+1}^b \\ -N_{j+1}^b & \nu_{j+1} K_{j+1}^b \end{bmatrix} \quad (\text{all operators evaluated at observation points } \mathbf{r} \text{ on } \Gamma_j). \end{aligned} \quad (10)$$

A general multi-layer integral formulation of the problem (1)–(2) can now be obtained in terms of these densities and operators. Indeed, as is shown in Appendix A, the fields within the layers admit the integral representations

$$\begin{aligned} u_1(\mathbf{r}) &= D_1^b[\varphi_1](\mathbf{r}) - \nu_1 S_1^b[\psi_1](\mathbf{r}) + u^{\text{inc}}(\mathbf{r}), \\ u_j(\mathbf{r}) &= D_j^b[\varphi_j](\mathbf{r}) - \nu_j S_j^b[\psi_j](\mathbf{r}) \\ &\quad - D_j^t[\varphi_{j-1}](\mathbf{r}) + S_j^t[\psi_{j-1}](\mathbf{r}), \quad j = 2, \dots, N - 1, \\ u_N(\mathbf{r}) &= -D_N^t[\varphi_{N-1}](\mathbf{r}) + S_N^t[\psi_{N-1}](\mathbf{r}) + u_N^{\parallel}(\mathbf{r}), \end{aligned} \quad (11)$$

in terms of the interface values (8). Therefore, evaluating $u_1 + u_2$ and $\partial u_1/\partial n + \partial u_2/\partial n$ on Γ_1 from the boundary values on Γ_1 of the expressions in (11) and their normal derivatives, and using the notations (9) and (10), we obtain the $j = 1$ interface equation

$$E_1 \phi_1 + T_1 [\phi_1] + R_1 [\phi_2] = \phi^{\text{inc}} \quad \text{on } \Gamma_1. \quad (12a)$$

A similar procedure yields the integral equations

$$E_j \phi_j + L_j [\phi_{j-1}] + T_j [\phi_j] + R_j [\phi_{j+1}] = \mathbf{0} \quad \text{on } \Gamma_j, \quad j = 2, \dots, N-2 \quad (12b)$$

and

$$E_{N-1} \phi_{N-1} + L_{N-1} [\phi_{N-2}] + T_{N-1} [\phi_{N-1}] = \phi^{\parallel} \quad \text{on } \Gamma_{N-1}. \quad (12c)$$

(Note that, of course, the calculations leading to equations (12) rely on the well-known jump relations for the single- and double-layer potentials and their normal derivatives [11].)

Remark 3.1. *In what follows equations (12) are expressed in terms of a single column vector function ϕ (defined on the Cartesian product $\Gamma = \prod_{j=1}^{N-1} \Gamma_j$ of the curves Γ_j) whose j -entry equals the density pair $\phi_j = [\varphi_j, \psi_j]^T : \Gamma_j \rightarrow \mathbb{C}^2$ for $j = 1, \dots, N-1$. We may thus write*

$$\phi = [\phi_1, \psi_1, \varphi_2, \psi_2, \dots, \varphi_{N-1}, \psi_{N-1}]^T : \Gamma \rightarrow \mathbb{C}^{2(N-1)}.$$

Similarly we define

$$\phi^{\text{inc}} = \left[u^{\text{inc}}|_{\Gamma_1}, \frac{\partial u^{\text{inc}}}{\partial n}|_{\Gamma_1}, 0, 0, \dots, 0, 0, u_N^{\parallel}|_{\Gamma_{N-1}}, \frac{\partial u_N^{\parallel}}{\partial n}|_{\Gamma_{N-1}} \right]^T : \Gamma \rightarrow \mathbb{C}^{2(N-1)}.$$

With a slight notational abuse we will write $\phi = [\phi_1, \phi_2, \dots, \phi_{N-1}]^T = [\phi_1, \psi_1, \varphi_2, \psi_2, \dots, \varphi_{N-1}, \psi_{N-1}]^T$. More generally, given arbitrary vectors $\mu_j = [\alpha_j, \beta_j]^T : \Gamma_j \rightarrow \mathbb{C}^2$ for $j = 1, \dots, N-1$ we will use the ‘‘block-vector’’ notation $\mu = [\mu_1, \mu_2, \dots, \mu_{N-1}]^T = [\alpha_1, \beta_1, \alpha_2, \beta_2, \dots, \alpha_{N-1}, \beta_{N-1}]^T : \Gamma \rightarrow \mathbb{C}^{2(N-1)}$.

Using the operators

$$\mathcal{E} = \begin{bmatrix} E_1 & & & & \\ & E_2 & & & \\ & & \ddots & & \\ & & & E_{N-1} & \end{bmatrix} \quad \text{and} \quad \mathcal{T}_\Gamma = \begin{bmatrix} T_1 & R_1 & & & \\ L_2 & T_2 & R_2 & & \\ & L_3 & \ddots & \ddots & \\ & & \ddots & \ddots & R_{N-2} \\ & & & L_{N-1} & T_{N-1} \end{bmatrix} \quad (13)$$

together with the notations introduced in Remark 3.1, equations (12) can be expressed in the form

$$\mathcal{E}\phi + \mathcal{T}_\Gamma[\phi] = \phi^{\text{inc}} \quad \text{on } \Gamma. \quad (14)$$

4 Windowed integral equations

Following [4], in this section we introduce rapidly-convergent windowed versions of the integral formulation (14). In order to do so we utilize the $(N-1) \times (N-1)$ block-diagonal matrix-valued window function $\mathcal{W}_A : \prod_{j=1}^{N-1} \Gamma_j \mapsto \mathbb{R}^{2(N-1) \times 2(N-1)}$ given by

$$\mathcal{W}_A(\mathbf{r}_1, \mathbf{r}_2, \dots, \mathbf{r}_{N-1}) = \begin{bmatrix} w_A(x_1) \mathbf{I} & & & \\ & w_A(x_2) \mathbf{I} & & \\ & & \ddots & \\ & & & w_A(x_{N-1}) \mathbf{I} \end{bmatrix}, \quad \mathbf{r}_j = (x_j, y_j) \in \Gamma_j, \quad (15)$$

in terms of the two-by-two identity matrix \mathbf{I} and the smooth window function

$$w_A(x) = \eta(x/A; c, 1), \quad (16)$$

where $0 < c < 1$ and where

$$\eta(t; t_0, t_1) = \begin{cases} 1, & |t| \leq t_0, \\ \exp\left(\frac{2e^{-1/u}}{u-1}\right), & t_0 < |t| < t_1, u = \frac{|t| - t_0}{t_1 - t_0}, \\ 0, & |t| > t_1. \end{cases} \quad (17)$$

Clearly η and w_A are infinitely differentiable compactly-supported functions of x and t , respectively. The support of the window function $w_A = w_A(x)$ as a function of $\mathbf{r} = (x, y) \in \mathbb{R}^2$ equals the set $[-A, A] \times \mathbb{R}$. Note that the parameter c , which controls the steepness of the rise of the window function w_A , is not displayed as part of the notation w_A .

(While different values A_j of the window-size A , $j = 1, \dots, N-1$, could in principle be used for the various layer interfaces and corresponding block entries in (15)—possibly utilizing smaller (resp. larger) values A_j in higher (resp. lower) frequency layers, and therefore reducing the overall number of unknowns required for the WGF method to produce a given accuracy. For simplicity, however, throughout this paper a single window-size value A is used for all the interfaces.)

In order to produce a windowed version of equation (14) we proceed in two stages. At first the integrand is multiplied by the window matrix \mathcal{W}_A and the equation is restricted to the windowed region $\Gamma_A = \{(\mathbf{r}_1, \dots, \mathbf{r}_{N-1}) \in \Gamma : \mathbf{r}_j = (x_j, y_j) \text{ and } w_A(x_j) \neq 0 \text{ for all } j\} \subset \mathbb{R}^{2(N-1)}$ —so that, moving the remainder of the windowed integral operator to the right-hand side and letting \mathcal{I} denote the identity matrix of dimension $2(N-1) \times 2(N-1)$, the exact relation

$$\mathcal{E}\phi + \mathcal{T}_\Gamma[\mathcal{W}_A\phi] = \phi^{\text{inc}} - \mathcal{T}_\Gamma[(\mathcal{I} - \mathcal{W}_A)\phi] \quad \text{on } \Gamma_A \quad (18)$$

results. Note that defining $\Gamma_{j,A} = \Gamma_j \cap \{w_A \neq 0\} = \Gamma_j \cap \{[-A, A] \times \mathbb{R}\}$ we have

$$\Gamma_A = \prod_{j=1}^{N-1} \Gamma_{j,A}. \quad (19)$$

A successful implementation of the WGF idea requires use of an accurate substitute for the quantity $\mathcal{T}_\Gamma[(\mathcal{I} - \mathcal{W}_A)\phi]$ throughout Γ_A , which does not depend on knowledge of the unknown density ϕ (cf. [4]). In order to obtain such an approximation we introduce an operator \mathcal{T}_P which is defined just like \mathcal{T}_Γ in (13) but in terms of potentials (6) and operators (7) given by integrals on the flat interfaces P_j depicted in Figure 1a. Since $(\mathcal{I} - \mathcal{W}_A)$ vanishes wherever Γ differs from $P = \prod_{j=1}^{N-1} P_j$, we clearly have $\mathcal{T}_\Gamma[(\mathcal{I} - \mathcal{W}_A)\phi] = \mathcal{T}_P[(\mathcal{I} - \mathcal{W}_A)\phi]$. Additionally, we consider the aforementioned scalar densities $\varphi_j^p = u_{j+1}^p|_{\Gamma_j}$ and $\psi_j^p = \partial u_{j+1}^p / \partial n|_{\Gamma_j}$ on P_j ($j = 1, \dots, N-1$) that are associated with the planarly layered medium P . As shown in [4], letting $[\phi^p]_j = [\varphi_j^p, \psi_j^p]^T$ ($j = 1, \dots, N-1$), substitution of ϕ by ϕ^p on the right-hand-side of (21) results in errors that decay super-algebraically fast as $A \rightarrow \infty$ within the subset

$$\tilde{\Gamma}_A = \Gamma_A \cap \prod_{j=1}^{N-1} \{(x_j, y_j) \in \Gamma_j : w_A(x_j) = 1\} \quad (20)$$

of Γ_A wherein the window function w_A equals one. Indeed, even though ϕ may differ significantly from ϕ^p , the corresponding integrated terms result in super-algebraically small errors, as it may be

checked via stationary phase analysis (see [4], for details). We thus obtain the super-algebraically-accurate windowed integral equation system

$$\mathcal{E}\phi^w + \mathcal{T}_\Gamma[\mathcal{W}_A\phi^w] = \phi^{\text{inc}} - \mathcal{T}_P[(\mathcal{I} - \mathcal{W}_A)\phi^p] \quad \text{on } \Gamma_A \quad (21)$$

which we re-express in the form

$$\mathcal{E}\phi^w + \mathcal{T}_\Gamma[\mathcal{W}_A\phi^w] = \phi^{\text{inc}} + \mathcal{T}_P[\mathcal{W}_A\phi^p] - \mathcal{T}_P[\phi^p] \quad \text{on } \Gamma_A. \quad (22)$$

As shown in what follows, the right-hand term $\mathcal{T}_P[\phi^p]$ in (22) can be expressed in closed form, and thus, using numerical integration over the bounded domain Γ_A to produce the term $\mathcal{T}_P[\mathcal{W}_A\phi^p]$, the complete right-hand side can be efficiently evaluated for any given $\mathbf{x} \in \Gamma_A$.

A closed-form expression for $\boldsymbol{\mu} = \mathcal{T}_P[\phi^p]$ (cf. Remark 3.1) can be obtained via an application of Green's formula: using (48) with $C = P_j$ ($j = 1, \dots, N-1$), equations (53) yield the desired relations:

$$\boldsymbol{\mu}_j = \delta_{1,j}\phi^{\text{inc}} + \delta_{N-1,j}\phi^{\parallel} - \begin{cases} \mathbf{E}_j \phi_j^p & \text{on } \Gamma_j \cap P_j, \\ \left[\begin{array}{c} u^p \\ \nabla u^p \cdot \mathbf{n} \end{array} \right] & \text{on } \Gamma_j \cap (D_j \cup D_{j+1}), \end{cases} \quad (23)$$

for $j = 1, \dots, N-1$, where $\delta_{i,j}$ denotes the Kronecker delta symbol.

As demonstrated in Section 7 through a variety of numerical examples, the vector density function ϕ^w , which is the solution of the windowed integral equation (22), converges super-algebraically fast to the exact solution ϕ of (14) within Γ_A^1 as the window size $A > 0$ increases. This observation can be justified via arguments analogous to those presented in [4].

Remark 4.1. *The difference $N_{j+1}^t - N_j^b$ of hypersingular operators that appears in the definition of the diagonal blocks \mathbb{T}_j of \mathcal{T}_Γ is in fact a weakly singular integral operators (cf. [11, Sec. 3.8]).*

5 Near-field evaluation

This section presents a super-algebraically accurate WGF approximation u^w of the solution u of (1)–(2) near the localized defects. In order to obtain this approximation we consider the “defect” field

$$u_j^d = u_j - \tilde{u}_j^p \quad \text{in } \Omega_j \quad (j = 1, \dots, N-1), \quad (24)$$

given by the difference between the total field u_j and the planar-structure total field

$$\tilde{u}_j^p(x, y) = A_j e^{ik_1 x} \left\{ e^{-ik_j y} + \tilde{R}_{j,j+1} e^{ik_j y (y+2d_j)} \right\} \quad \text{in } \Omega_j, \quad 1 \leq j \leq N. \quad (25)$$

Note that \tilde{u}_j^p is given in Ω_j by the expressions on the right-hand side of equation (3).

Subtracting the integral representation

$$\begin{aligned} \tilde{u}_1^p(\mathbf{r}) &= D_1^b[\tilde{\varphi}_1^p + f_1](\mathbf{r}) - \nu_1 S_1^b[\tilde{\psi}_1^p + g_1](\mathbf{r}) + u^{\text{inc}}(\mathbf{r}), \\ \tilde{u}_j^p(\mathbf{r}) &= D_j^b[\tilde{\varphi}_j^p + f_j](\mathbf{r}) - \nu_j S_j^b[\tilde{\psi}_j^p + g_j](\mathbf{r}) \\ &\quad - D_j^t[\tilde{\varphi}_{j-1}^p](\mathbf{r}) + S_j^t[\tilde{\psi}_{j-1}^p](\mathbf{r}), \quad j = 2, \dots, N-1, \\ \tilde{u}_N^p(\mathbf{r}) &= -D_N^t[\tilde{\varphi}_{N-1}^p](\mathbf{r}) + S_N^t[\tilde{\psi}_{N-1}^p](\mathbf{r}) + u_N^{\parallel}(\mathbf{r}), \end{aligned} \quad (26)$$

—which follows as equation (53) is applied to \tilde{u}_j^p —from the integral representation (11) we obtain the exact integral relations

$$\begin{aligned}
u_1^d(\mathbf{r}) &= D_1^b[\varphi_1 - \tilde{\varphi}_1^p - f_1](\mathbf{r}) - \nu_1 S_1^b[\psi_1 - \tilde{\psi}_1^p - g_1](\mathbf{r}), \\
u_j^d(\mathbf{r}) &= D_j^b[\varphi_j - \tilde{\varphi}_j^p - f_j](\mathbf{r}) - \nu_j S_j^b[\psi_j - \tilde{\psi}_j^p - g_j](\mathbf{r}) \\
&\quad - D_j^t[\varphi_{j-1} - \tilde{\varphi}_{j-1}^p](\mathbf{r}) + S_j^t[\psi_{j-1} - \tilde{\psi}_{j-1}^p](\mathbf{r}), \quad j = 2, \dots, N-1, \\
u_N^d(\mathbf{r}) &= -D_N^t[\varphi_{N-1} - \tilde{\varphi}_{N-1}^p](\mathbf{r}) + S_N^t[\psi_{N-1} - \tilde{\psi}_{N-1}^p](\mathbf{r})
\end{aligned} \tag{27}$$

for the defect fields. These relations can be used to evaluate the defect fields u_j^d in terms of the solution $\phi_j = [\varphi_j, \psi_j]^T$ of the integral equation (14) together with the planar-structure total fields

$$\tilde{\phi}_j^p = [\tilde{\varphi}_j^p, \tilde{\psi}_j^p]^T, \quad \text{where} \quad \tilde{\varphi}_j^p = \tilde{u}_{j+1}^p|_{\Gamma_j} \quad \text{and} \quad \tilde{\psi}_j^p = \frac{\partial \tilde{u}_{j+1}^p}{\partial n} \Big|_{\Gamma_j}, \tag{28}$$

and the jumps

$$\boldsymbol{\psi}_j = [f_j, g_j]^T, \quad \text{where} \quad f_j = \tilde{u}_j^p - \tilde{u}_{j+1}^p \quad \text{and} \quad g_j = \frac{1}{\nu_j} \frac{\partial \tilde{u}_j^p}{\partial n} - \frac{\partial \tilde{u}_{j+1}^p}{\partial n} \quad \text{on} \quad \Gamma_j. \tag{29}$$

Note that, importantly, for each j , $1 \leq j \leq N$, the functions f_j and g_j vanish outside the j -th portion $\Gamma_j \setminus \Pi_j$ of the boundary of the localized defects.

Relying on the WGF solutions ϕ^w of equation (22) and applying a windowing procedure similar to the one used in the previous section, a highly-accurate approximation to the defect near-fields (27) results. In detail, substitution of φ_j by $w_A \varphi_j^w + (1 - w_A) \tilde{\varphi}_j^p$ and ψ_j by $w_A \psi_j^w + (1 - w_A) \tilde{\psi}_j^p$ in (27) yields the approximate expressions

$$\begin{aligned}
u_1^{d,w}(\mathbf{r}) &= D_1^b[w_A(\varphi_1^w - \tilde{\varphi}_1^p) - f_1] - \nu_1 S_1^b[w_A(\psi_1^w - \tilde{\psi}_1^p) - g_1], \\
u_j^{d,w}(\mathbf{r}) &= D_j^b[w_A(\varphi_j^w - \tilde{\varphi}_j^p) - f_j] - \nu_j S_j^b[w_A(\psi_j^w - \tilde{\psi}_j^p) - g_j] \\
&\quad - D_j^t[w_A(\varphi_{j-1}^w - \tilde{\varphi}_{j-1}^p)] + S_j^t[w_A(\psi_{j-1}^w - \tilde{\psi}_{j-1}^p)], \quad j = 2, \dots, N-1, \\
u_N^{d,w}(\mathbf{r}) &= -D_N^t[w_A(\varphi_{N-1}^w - \tilde{\varphi}_{N-1}^p)] + S_N^t[w_A(\psi_{N-1}^w - \tilde{\psi}_{N-1}^p)],
\end{aligned} \tag{30}$$

for the defect field u_j^d . The desired approximation u_j^w for the total field u_j then follows from (24):

$$u_j^w = \tilde{u}_j^p + u_j^{d,w} \quad \text{in} \quad \Omega_j \quad (j = 1, \dots, N). \tag{31}$$

Formulae (31) provide super-algebraically accurate approximations of the total near-fields within the region

$$\tilde{\Omega}_A = \bigcup_{j=1}^N \Omega_j \cap \{\mathbf{r} \in \mathbb{R}^2 : w_A(x) = 1\} \tag{32}$$

containing the localized defects—with uniformly small errors, as $A \rightarrow \infty$, within every bounded subset of $\tilde{\Omega}_A$. A theoretical discussion in these regards (for the two-layer case) can be found in [4] (see e.g. Remark 4.1 in that reference).

6 Far-field evaluation

As indicated in the previous section, formulae (30)–(31) only provide uniformly accurate approximations within bounded subsets of $\tilde{\Omega}_A$. But, once accurate defect fields $u_j^{d,w}$ ($j = 1, \dots, N$) have been obtained within $\tilde{\Omega}_A$, correspondingly accurate far-field values for the solution u can be obtained by applying certain Green-type formulae on a bounding curve S , such as the one depicted in Figure 2, which encloses all of the local defects, and which is contained within $\tilde{\Omega}_A$. In detail, defining the defect field $u^d = u^d(\mathbf{r})$ to equal $u_j^d(\mathbf{r})$ for $\mathbf{r} \in \Omega_j$ ($j = 1, \dots, N$), use of a Green identity based on the N -layer Green function H over the region exterior to S leads to the integral representation [24, Lemma 4.2.6]

$$u^d(\mathbf{r}) = \int_S \left\{ \frac{\partial H}{\partial n_{\mathbf{r}'}}(\mathbf{r}, \mathbf{r}') u^d(\mathbf{r}') - H(\mathbf{r}, \mathbf{r}') \frac{\partial u^d}{\partial n}(\mathbf{r}') \right\} ds_{\mathbf{r}'}, \quad (33)$$

which is valid for \mathbf{r} everywhere outside S . Note that the necessary values of u_j^d and their normal derivatives on S can be computed by means of (31)—since, by construction, S lies inside the region where (31) provides an accurate approximation of the field u_j^d .

The far-field approximation u^f of the defect field u^d as $\mathbf{r} \rightarrow \infty$ in any direction is then obtained by replacing the layer Green function H and its normal derivative $\partial H / \partial n_{\mathbf{r}'}$ in (33) by the respective first-order $|\mathbf{r}| \rightarrow \infty$ asymptotic expansions H^f and $\partial H^f / \partial n_{\mathbf{r}'}$ —which can be obtained for the N -layer case (as illustrated in [2, 8, 24, 4, 3] for $N = 2$ and below in this section for $N = 3$) by means of the method of steepest descents. (The fact that the far field of the function $\partial H / \partial n_{\mathbf{r}'}$ coincides with $\partial H^f / \partial n_{\mathbf{r}'}$ can be verified by direct inspection of these two quantities.) The far field u^f is thus given by

$$u^f(\mathbf{r}) = \int_S \left\{ \frac{\partial H^f}{\partial n_{\mathbf{r}'}}(\mathbf{r}, \mathbf{r}') u^d(\mathbf{r}') - H^f(\mathbf{r}, \mathbf{r}') \frac{\partial u^d}{\partial n}(\mathbf{r}') \right\} ds_{\mathbf{r}'}. \quad (34)$$

It is important to note that, unlike the layer Green function H itself, the corresponding far-field H^f and its normal derivative can be evaluated inexpensively by means of explicit expressions.

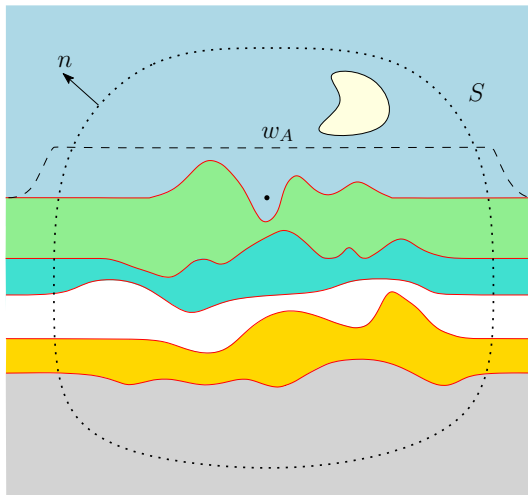


Figure 2: Curve S in (33).

As an example we sketch here the calculation of the far-field H^f for a slab—that is, a three-layer medium with wavenumbers k_j , $j = 1, 2, 3$ where $k_1 = k_3$ —in two-dimensional space. We

assume the case $k_2 > k_1$ for which the slab can sustain guided modes that propagate along the x -axis. In order to evaluate H^f we first note that, for a source point $\mathbf{r}' = (x', y') \in D_j$ and a target point $\mathbf{r} = (r \cos \theta, r \sin \theta) \in D_1$ ($\theta \in [0, \pi]$), the layer Green function H is given by the contour integral [2, 8, 24, 3]

$$H_j(\mathbf{r}, \mathbf{r}') = \frac{1}{4\pi} \int_{SC} \frac{p_j(\xi, \mathbf{r}')}{q(\xi)} e^{|\mathbf{r}|\phi(\xi)} d\xi. \quad (35)$$

Here, letting $\gamma_j(\xi) = \sqrt{\xi^2 - k_j^2}$, $j = 1, 2, 3$, we have set

$$\phi(\xi) = i\xi \cos \theta - \gamma_1(\xi) \sin \theta, \quad (36a)$$

$$p_1(\xi, \mathbf{r}') = \left\{ R_{12}(\xi) + R_{23}(\xi) e^{-2\gamma_2(\xi)d_2} \right\} \frac{e^{-i\xi x' - \gamma_1(\xi)y'}}{\gamma_1(\xi)} \quad (36b)$$

$$p_2(\xi, \mathbf{r}') = \{1 - R_{12}(\xi)\} \left\{ 1 + R_{23}(\xi) e^{-2\gamma_2(\xi)(d_2 + y')} \right\} \frac{e^{-i\xi x' + \gamma_2(\xi)y'}}{\gamma_2(\xi)} \quad (36c)$$

$$p_3(\xi, \mathbf{r}') = \{1 - R_{12}(\xi)\} \{1 - R_{23}(\xi)\} e^{-\gamma_2(\xi)d_2} \frac{e^{-i\xi x' + \gamma_3(\xi)(y' + d_2)}}{\gamma_3(\xi)} \quad (36d)$$

$$q(\xi) = 1 + R_{12}(\xi)R_{23}(\xi) e^{-2\gamma_2(\xi)d_2}, \quad (36e)$$

and

$$R_{ij}(\xi) = \frac{\gamma_i(\xi) - \nu_i \gamma_j(\xi)}{\gamma_i(\xi) + \nu_i \gamma_j(\xi)}, \quad i, j = 1, 2, 3. \quad (36f)$$

The determination of physically admissible branches of the functions $\gamma_j(\xi) = \sqrt{\xi^2 - k_j^2} = \sqrt{\xi - k_j} \sqrt{\xi + k_j}$ requires adequate selection of branch cuts. Relevant branches, which must be selected to insure the Green function satisfies outgoing radiation condition for the layered structure, are given by $-3\pi/2 \leq \arg(\xi - k_j) < \pi/2$ for $\sqrt{\xi - k_j}$ and $-\pi/2 \leq \arg(\xi + k_j) < 3\pi/2$ for $\sqrt{\xi + k_j}$. The branch cut stemming from the point $\xi = k_1 = k_3$ is in fact the only branch cut in the domain of definition of the functions $p_j(\xi, \mathbf{r}')/f(\xi)$ ($j = 1, 2, 3$), as it can be shown that these are even functions of γ_2 [8]. The branch cuts and Sommerfeld contour SC utilized in (35) are depicted in Figure 3.

As suggested above, in order to obtain the far-field form of the layer Green function H^f we resort to the method of steepest descents [2]. Analysis of the phase function ϕ (36a) readily shows that there is only one saddle point on the real axis at $\xi_0 = k_1 \cos \theta$ and that the path of steepest descent SD that passes through that point, which is given by the expression $\text{Im} \phi(\xi) = k_1$, also intersects the real axis at $\xi = k_1 / \cos \theta$. Furthermore, from the definition of the function γ_1 it can be shown that

$$\text{Im} \xi = \frac{|\cos \theta|}{\sin \theta} \text{Re} \xi - \frac{k_1}{\sin \theta} \quad \text{as } |\xi| \rightarrow \infty,$$

for ξ on SD . This information suffices to sketch the paths of steepest descent that are displayed in Figure 3.

In order to produce asymptotic expansions of the integrals (35) we then proceed to deform the Sommerfeld contour SC to the steepest descent contour SD (Figure 3). Considering the saddle point at ξ_0 and taking into account the poles of the integrand $p_j(\xi, \mathbf{r}')/q(\xi)$ at the points ξ_p which are enclosed by the curves SD and SC , we obtain the following expression for the far-field form of

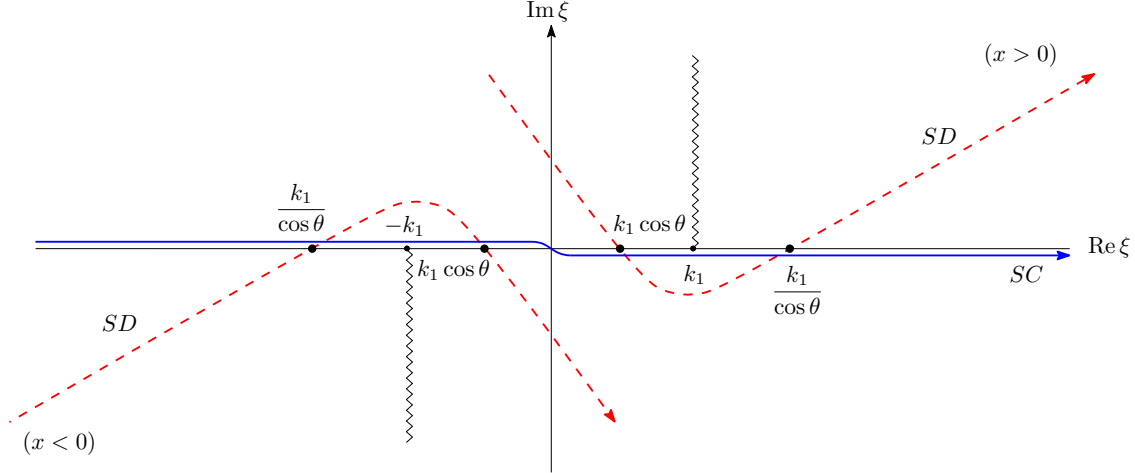


Figure 3: Sommerfeld contour SC used in (35) (solid blue curve) and related steepest descent path SD (dashed red curve).

the Green function for the two-dimensional slab:

$$\begin{aligned}
 H^f(\mathbf{r}, \mathbf{r}') &= \frac{i}{2} \sum_{\xi_p \in I} \text{Res}_{\xi=\xi_p} \left(\frac{p_j(\xi, \mathbf{r}')}{q(\xi)} e^{|\mathbf{r}|\phi(\xi)} \right) + \\
 &\quad \frac{1}{4\pi} \frac{p_j(\xi_0, \mathbf{r}')}{q(\xi_0)} \sqrt{\frac{2\pi}{|\mathbf{r}|\phi''(\xi_0)}} e^{|\mathbf{r}|\phi(\xi_0) - i\pi/4} + O(|\mathbf{r}|^{-3/2}), \quad (\mathbf{r}' \in D_j)
 \end{aligned} \tag{37}$$

as $|\mathbf{r}| \rightarrow \infty$. Note that for $\cos \theta > 0$ (resp. $\cos \theta < 0$) only the real poles contained in the set $I = (0, k_1 \cos \theta) \cup (k_1 / \cos \theta, \infty)$ (resp. $I = (-\infty, k_1 / \cos \theta) \cup (k_1 \cos \theta, 0)$) produce contributions which do not decay exponentially.

Clearly, as indicated above, the far field asymptotics H^f of the layer Green function H , and thus its normal derivative, can be evaluated inexpensively by means of a simple explicit expressions.

7 Numerical examples

This section presents a set of two- and three-dimensional numerical examples that demonstrate the character of the proposed multi-layer WGF methodology. For the sake of definiteness a window function w_A (16) with $c = 0.7$ was used in all cases. Numerical errors were evaluated by resorting to numerical-convergence studies and/or increases in the window-size A . As additional references, in some cases adequately accurate solutions obtained by the Sommerfeld layer-Green-function (LGF) method [23, 24] (with accuracy evaluated by means of convergence studies) were used to evaluate the accuracy of the WGF approach. Brief indications will be provided when necessary to indicate which method is being used in each case. The two-dimensional results were obtained via solution of the integral equation system (22) by means of the Nyström method described in [10, Section 3.5]. The three-dimensional solutions, in turn, were obtained by means of the algorithm presented in [5].

Our first example concerns the structure depicted in the left portion of Figure 4, in which semi-circular defects of radii $a = 1$ are placed at the planar interfaces $P_1 = \mathbb{R} \times \{0\}$ and $P_2 = \mathbb{R} \times \{-3/2\}$ of a three-layer medium with wavenumbers $k_1 = 10$, $k_2 = 20$ and $k_3 = 30$. The right portion of Figure 4

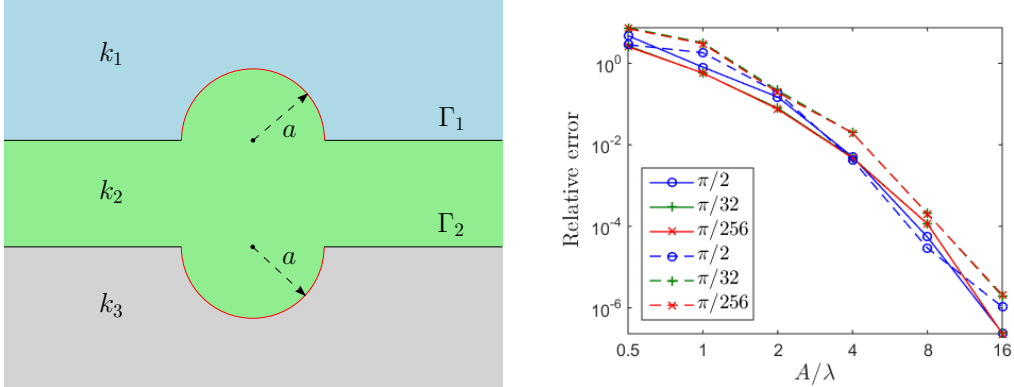


Figure 4: Left. Structure utilized in the numerical examples presented in Section 7. Right. Relative errors in log-log scale in the integral densities resulting from numerical solution of (22) for the structure depicted on the left panel, by means of the WGF method, for various window sizes and angles of incidence—including extremely shallow incidences. The WGF method computes integral densities with super-algebraically high accuracy uniformly for all incidences.

displays the maximum relative errors (in log-log scale) in the total field produced by the WGF method on the surface of the semi-circular defects (the curves marked in red in Figure 4 left) for various windows sizes $A > 0$ and incidences α . The number of quadrature points was selected in such a way that for any given $A > 0$ the Nyström discretization error in the integral equation solution is not larger than 10^{-9} . The WGF solution obtained for $A = 32\lambda$ is utilized as the reference for the error estimation. As it can be inferred from the error curves displayed in Figure 4, super-algebraic convergence is observed as A increases. In particular, these results demonstrate the uniformly fast convergence exhibited by the WGF method as the incidence angles approach grazing.

κ	WGF method					LGF method				
	2	4	8	16	32	2	4	8	16	32
Number of unknowns	1232	1272	1348	1496	1800	68	148	300	596	1204
Matrix construction (s)	3.44	3.53	3.98	5.78	7.29	6.49	22.15	82.86	319.46	1900

Table 1: Computing times required by the WGF and LGF methods to construct the system matrices for the numerical solution of the problem of scattering of a plane-wave by a semi-circular cavity or radius $a = 1$ on a three-layer medium with wavenumbers $k_1 = \kappa$, $k_2 = 2\kappa$ and $k_3 = 3\kappa$, with $\kappa = 2^j$, $j = 1, \dots, 5$. All the two-dimensional runs reported in this paper were performed using a Matlab implementation of our algorithms in a MacBook Air laptop (early 2014 model).

In order to compare the computational cost of the LGF method [23] and proposed WGF method for a given accuracy, we consider a planar three-layer structure similar to those considered previously, but now containing only one surface defect: a semi-circular cavity of radius $a = 1$ at P_1 . (The use of a single defect reduces somewhat the LGF cost which seemed inordinately large for the two-defect problem.) A plane-wave u^{inc} with $\alpha = -\pi/6$ illuminates the structure. Five sets of wavenumbers given by $k_1 = \kappa$, $k_2 = 2\kappa$ and $k_3 = 3\kappa$ with $\kappa = 2^j$, $j = 1, \dots, 5$ are considered. The resulting problems of scattering are then solved by employing a Nyström discretization of the WGF

equations (22), and a numerical version of (31) is used to evaluate near-fields. The same problem of scattering is then solved, with a relative error not larger than 10^{-4} , by means of a generalization to the present three-layer case, of the two-layer LGF method presented in [23] (see also [24]). The reference solution used to estimate the accuracy of the LGF solution is obtained by solving the resulting LGF integral equation with an error not larger 10^{-9} (this accuracy is achieved by utilizing a large number of Nyström quadrature points and evaluating the layer Green function with an error not larger than 10^{-10}).

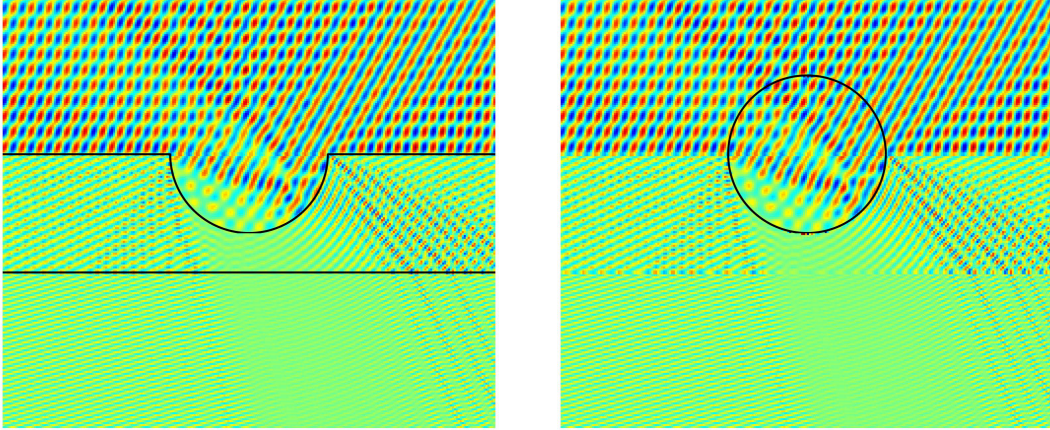


Figure 5: Real part of the total near fields obtained (with errors of the order of 10^{-4}) by means of the WGF (left) and LGF (right) methods for the problem of scattering of a plane wave by a semi-circular cavity of radius $a = 1$ on the top interface of a three-layer medium with wavenumbers $k_1 = 32$, $k_2 = 64$ and $k_3 = 96$ and incidence angle $\alpha = -\pi/6$. The respective integral-equation curves are shown in black. The WGF solution with $A = 16\lambda$ (resp. the LGF solution) was produced in total computing time of 62 secs (resp. $7.8 \cdot 10^4$ secs).

Table 1 displays the computing times needed by both methods to construct the system matrices. In order to allow for a fair comparison of the computing times and the field values on the surface defect, the same set of quadrature points is utilized to discretize the currents on the surface of the cavity in each case. The number of quadrature points was increased in direct proportion to the value of κ . The maximum of the absolute value of the difference between the LGF and WGF solutions (using $A = 8\lambda$) on the surface of the defect is no larger than 10^{-4} in all the examples considered. Remarkably, in the $\kappa = 32$ case the proposed WGF method is 260 times faster than the LGF method.

Figure 5 presents a comparison of the near fields obtained by means of the WGF and LGF methods for some of the test cases considered in Table 1. The first and second columns in Figure 5 display the real-part of the total near-fields produced by the WGF method (1st column) and by the LGF method (2nd column) respectively for $\kappa = 32$. The fields are evaluated in the rectangular region $[-3, 3] \times [-7/2, 2]$ at an uniform grid of 280×200 points. Note that, as it follows from consideration of the figure captions, the WGF near field evaluation procedure is up to 1200 times faster than the corresponding LGF near field evaluation procedure—in spite of the fact that a (larger) window size $A = 16\lambda$ had to be used to produce accurate near fields throughout the plotted region.

Figure 6, in turn, compares the far-field patterns

$$u_\infty(\hat{\mathbf{r}}) = \lim_{|\mathbf{r}| \rightarrow \infty} \sqrt{|\mathbf{r}|} e^{-ik_1|\mathbf{r}|} u(|\mathbf{r}|\hat{\mathbf{r}}), \quad \hat{\mathbf{r}} = \frac{\mathbf{r}}{|\mathbf{r}|} = (\cos \theta, \sin \theta), \quad \theta \in (0, \pi), \quad (38)$$

produced by the WGF and LGF algorithms for a semi-circular cavity in a three-layer medium with wavenumbers $k_1 = k_3 = 10$ and $k_2 = 15$. The WGF far-field pattern (blue solid line) was obtained by letting $u = u^f$ in (38), where u^f is given by (34) with WGF defect fields $u^d = u_j^{d,w}$ in Ω_j , $j = 1, \dots, N$ (equation (31)). The corresponding LGF far-field pattern (red dots) was obtained on the basis of a highly accurate LGF solution together with the far-field asymptotics of the layer Green function [23]. We have verified that, as expected, the accuracy of the WGF far-field patterns is comparable to the accuracy of the corresponding defect fields $u_j^{d,w}$ within the region $\tilde{\Omega}_A$.

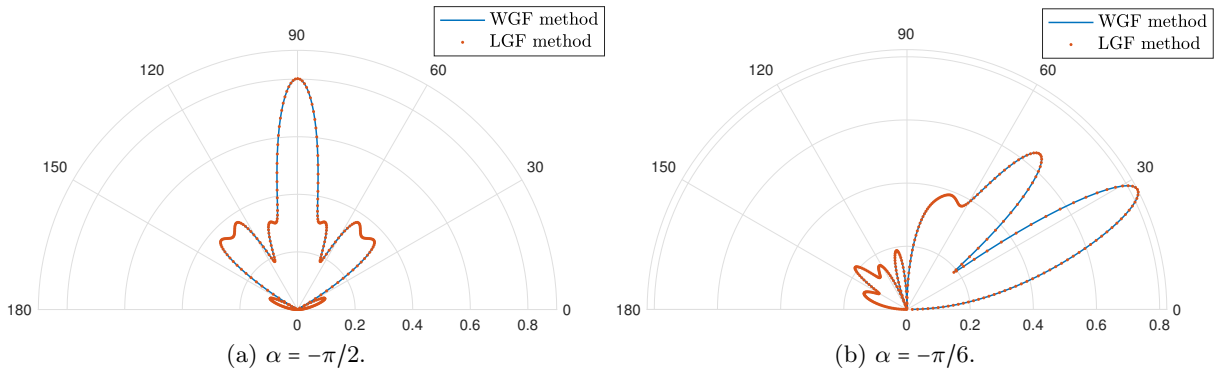


Figure 6: WGF (blue solid line) and LGF (red dotted line) far-field patterns obtained for the problems of scattering of a semi-circular cavity in a slab with wavenumbers $k_1 = k_3 = 10$ and $k_2 = 15$ for two different incidence angles.

Figure 7 displays near fields resulting from the WGF method, with window size $A = 12\lambda$, for a structure consisting of nested circular surface defects in a nine-layer medium with planar interfaces $P_j = \mathbb{R} \times \{(j-1)/5\}$, $j = 1, \dots, 8$. The corresponding wavenumbers are $k_{2j-1} = 15$ for $j = 1, \dots, 5$ and $k_{2j} = 30$ for $j = 1, \dots, 4$. The structure is illuminated by plane-waves with two different incidence angles. A 112-second overall computing time sufficed to evaluate each one of the two near fields displayed. Note the resonance that takes place in the third upper and lower rings in Figure 7 right.

Figure 8, finally, presents applications of the WGF methodology to the problem of scattering by three-dimensional structures in presence of layer media. The two-dimensional descriptions presented in Sections 2 through 6 extend directly to the present three-dimensional context.

Acknowledgements

This work was supported by NSF and AFOSR through contracts DMS-1411876 and FA9550-15-1-0043, and by the NSSEFF Vannevar Bush Fellowship under contract number N00014-16-1-2808.

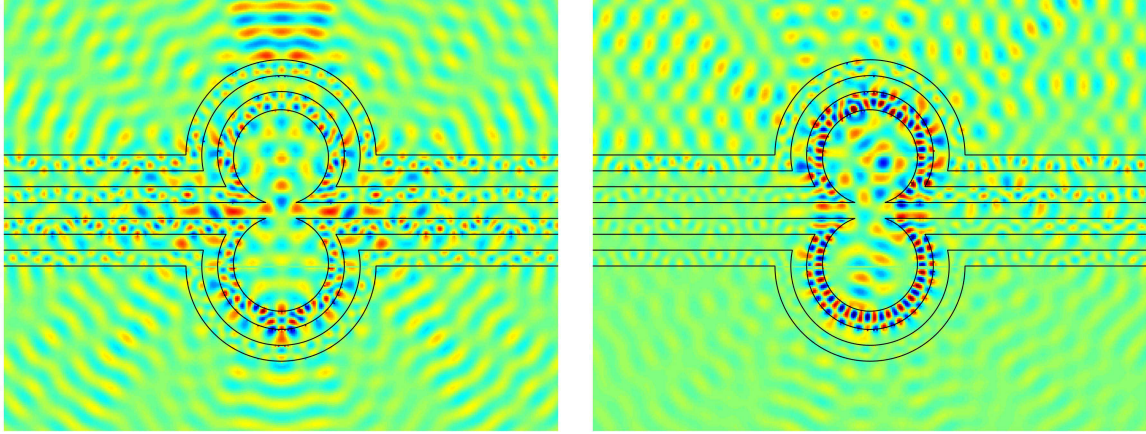


Figure 7: Real part of the total field for the problem of scattering of a plane wave impinging on a layered medium composed by 9 layers: $k_{2j-1} = 15$, $j = 1, \dots, 5$ and $k_{2j} = 30$, $j = 1, \dots, 4$ and $P_j = \mathbb{R} \times \{(j-1)/5\}$, $j = 1, \dots, 8$.

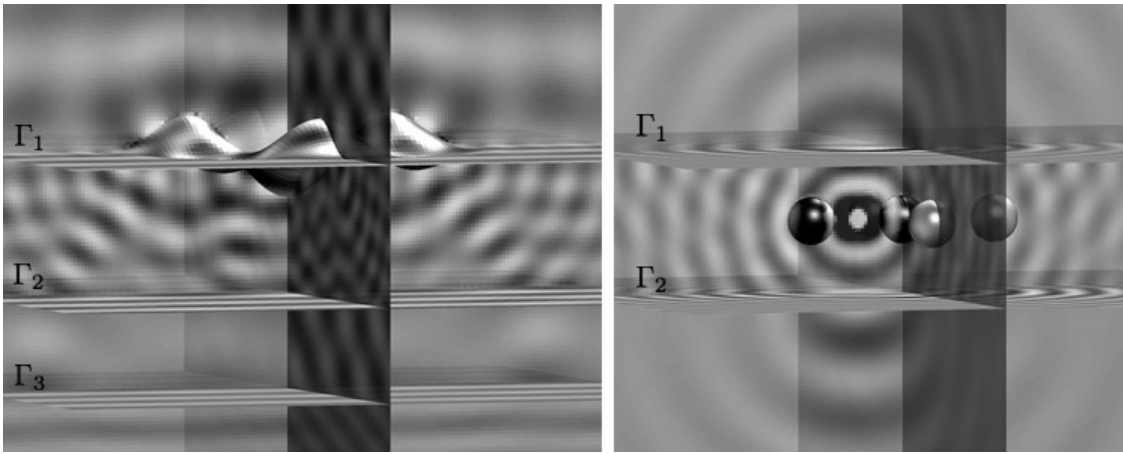


Figure 8: Three-dimensional total fields (real parts shown) produced by the WGF approach. Left. Scattering of a plane-wave by a surface defect in a four-layer medium with wavenumbers $k_1 = k_3 = 4$ and $k_2 = k_4 = 8$. Right. Scattering of a point-source field by an array of five spheres in a three-layer medium with wavenumbers $k_1 = k_3 = 4$ and $k_2 = 8$. The absolute errors in the surface fields displayed are no larger than $4 \cdot 10^{-4}$ for corresponding maximum fields of order one.

A Appendix: Integral representation based on non-windowed free-space Green functions

This section presents an integral representation formula, based on the *free-space Green function*, for fields of the form $v(\mathbf{r}) = v_j(\mathbf{r})$ for $\mathbf{r} \in \Omega_j$, $j = 1, \dots, N$, where, letting u_j^d and \tilde{u}_j^p be defined in (24) and (25), respectively, we have either

$$v_j = u_j^d + \tilde{u}_j^p, \quad v_j = u_j^d \quad \text{or} \quad v_j = \tilde{u}_j^p \quad \text{in} \quad \Omega_j. \quad (39)$$

The presentation is restricted to two-dimensional configurations. A related (modified) representation, which can similarly be utilized for all purposes necessary in this paper, can be ob-

tained analogously—albeit with certain additional considerations, as detailed in [15] in the three-dimensional sound-hard case; cf. also [14]. For simplicity, the presentation is further restricted to three-layer structures, but the extension to N -layer structures is straightforward.

Our derivations utilize three local polar-coordinate systems, each one of which is associated with one of the layers Ω_j . These coordinate systems are centered at $(0, -d_1)$, $(0, -(d_1 + d_2)/2)$ and $(0, -d_2)$ and, thus, the radial variables are given by

$$r_1 = \sqrt{x^2 + (y + d_1)^2}, \quad r_2 = \sqrt{x^2 + (y + (d_1 + d_2)/2)^2}, \quad \text{and} \quad r_3 = \sqrt{x^2 + (y + d_2)^2}, \quad (40)$$

in terms of the global Cartesian coordinates x and y , as illustrated in Figure 9.

Additionally, some of the subsequent derivations utilize the decomposition

$$\tilde{u}_j^p = u_j^\uparrow + u_j^\downarrow \quad \text{in} \quad \Omega_j, \quad (41)$$

where letting $k_{1x} = k_1 \cos \alpha$ and $k_{jy} = \sqrt{k_j^2 - k_{1x}^2}$, the up-going and down-going plane-waves u_j^\uparrow and u_j^\downarrow are given by

$$u_j^\uparrow(\mathbf{r}) = p_j e^{ik_{1x}x + ik_{jy}y} \quad \text{and} \quad u_j^\downarrow(\mathbf{r}) = q_j e^{ik_{1x}x - ik_{jy}y}, \quad (42)$$

respectively. Here the constants $p_j = e^{2ik_{jy}d_j} A_j \tilde{R}_{j,j+1}$ and $q_j = A_j$ are expressed in terms of the amplitudes A_j and the generalized reflection coefficients $\tilde{R}_{j,j+1}$ defined in (4) and (5). Note that $u_1^\downarrow = u^{\text{inc}}$ and $u_3^\uparrow = 0$. The defect field v_j^d , on the other hand, is given by [16, 20]

$$v_j^d = \begin{cases} v_j^{\text{rad}} + v_j^{\text{gui}} & \text{in } \Omega_j, \quad j = 1, 3, \\ v_2^{\text{gui}} & \text{in } \Omega_2, \quad j = 2, \end{cases} \quad (43)$$

in terms of radiative and guided wave fields v_j^{rad} and v_j^{gui} which, letting $\beta_2 = 1$ and $\beta_j = 2/3$ for $j = 1, 3$ (see (40)), verify

$$\lim_{r_j \rightarrow \infty} \sqrt{r_j} \left(\frac{\partial v_j^{\text{rad}}}{\partial r_j} - ik_j v_j^{\text{rad}} \right) = 0, \quad j = 1, 3, \quad (44)$$

and

$$\begin{cases} v_j^{\text{gui}}(\mathbf{r}) = \sum_{m=1}^{M_j} \alpha_j^m v_j^m(\mathbf{r}) + O(r_j^{-\beta_j}), \\ \left| \frac{\partial v_j^{\text{gui}}}{\partial r_j} - i \sum_{m=1}^{M_j} \alpha_j^m \xi_j^m v_j^m \right| = O(r_j^{-\beta_j}) \end{cases} \quad \text{as } r_j \rightarrow \infty, \quad (j = 1, 2, 3). \quad (45)$$

Here v_j^m denote the guided modes

$$v_j^m(\mathbf{r}) = \begin{cases} \{a_2^m \cosh(\gamma_2^m y) + b_2^m \sinh(\gamma_2^m y)\} e^{i|x|\xi_2^m}, & j = 2, \\ e^{-\gamma_j^m |y|} e^{i|x|\xi_j^m}, & j = 1, 3, \end{cases} \quad (46)$$

which are expressed in terms of the so-called propagation constants $\xi_j^m > 0$, and $\gamma_j^m = \sqrt{(\xi_j^m)^2 - k_j^2}$, $m = 1, \dots, M_j$. The propagation constants ξ_j^m equal the real poles (sometimes called surface wave poles [9, 7]) of the corresponding three-layer Green function in spectral form. The condition for the existence of the propagative modes in the inner layer Ω_2 is $k_1 < \xi_2^m < k_2$. For the outer layer Ω_1

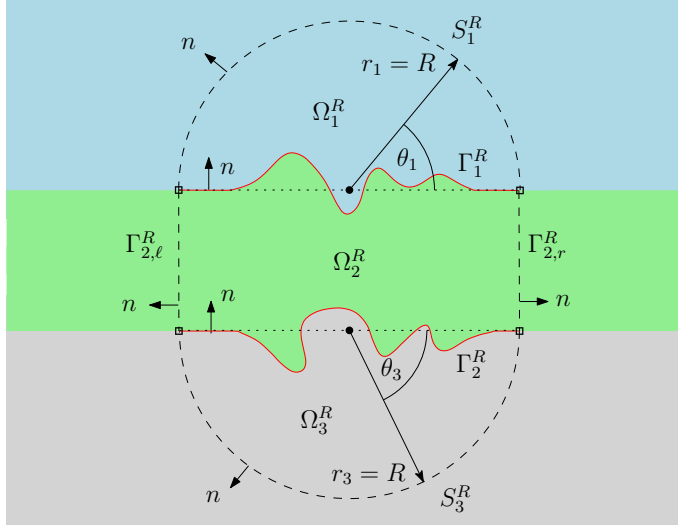


Figure 9: Depiction of the various domains, boundaries and variables involved in the derivation of the integral representation formula (51).

(resp. Ω_3), on the other hand, we have $\xi_1^m = \xi_2^m$ (resp. $\xi_3^m = \xi_2^m$) and the guided-mode condition is $\xi_1^m > k_1$ (resp. $\xi_3^m > k_3$). Thus v_1^m (resp. v_3^m) corresponds to a surface wave that travels along the interface Γ_1 (resp. Γ_2) and decays exponentially fast towards the interior of Ω_1 (resp. Ω_3).

We are now in a position to derive the desired integral representation for the total fields v_j in (39). Our derivations consider at first the bounded domains

$$B_R = ((-R, R) \times (-d_2, -d_1)) \cup \{(x, y) : r_1 < R\} \cup \{(x, y) : r_3 < R\} \quad (47)$$

where $R > 0$ is large enough that B_R contains all of the surface defects, as illustrated in Figure 9. Our bounded-domain calculations use the curves $\Gamma_{2,\ell}^R$, $\Gamma_{2,r}^R$, S_1^R and S_3^R and corresponding normals n , as depicted in Figure 9. In order to facilitate repeated use of Green's third identity in our derivations we follow [14] and, letting $G_{k_j}(\mathbf{r}, \mathbf{r}') = \frac{i}{4} H_0^{(1)}(k_j |\mathbf{r} - \mathbf{r}'|)$ we define, for a given curve C ,

$$I_j[v; C](\mathbf{r}) = \int_C \left\{ \frac{\partial G_{k_j}}{\partial n_{\mathbf{r}'}}(\mathbf{r}, \mathbf{r}') v(\mathbf{r}') - G_{k_j}(\mathbf{r}, \mathbf{r}') \frac{\partial v}{\partial n}(\mathbf{r}') \right\} ds_{\mathbf{r}'}. \quad (48)$$

In what follows, finally, we make frequent use of the $|\mathbf{r}'| \rightarrow \infty$ asymptotic relations

$$\begin{aligned} G_k(\mathbf{r}, \mathbf{r}') &= \frac{i e^{-i\pi/4}}{\sqrt{8\pi k |\mathbf{r}'|}} e^{ik(|\mathbf{r}'| - \mathbf{r} \cdot \hat{\mathbf{r}}')} \{1 + O(|\mathbf{r}'|^{-1})\}, \\ \nabla_{\mathbf{r}'} G_k(\mathbf{r}, \mathbf{r}') &= -\frac{\sqrt{k} e^{-i\pi/4}}{\sqrt{8\pi |\mathbf{r}'|}} e^{ik(|\mathbf{r}'| - \mathbf{r} \cdot \hat{\mathbf{r}}')} \hat{\mathbf{r}}' \{1 + O(|\mathbf{r}'|^{-1})\} \end{aligned} \quad \left(\hat{\mathbf{r}}' = \frac{\mathbf{r}'}{|\mathbf{r}'|} \right) \quad (49)$$

that follow directly from the corresponding asymptotic expressions for the Hankel function [17] together with easily verified identity $|\mathbf{r} - \mathbf{r}'| = |\mathbf{r}'| - \mathbf{r}' \cdot \mathbf{r} / |\mathbf{r}'| + O(|\mathbf{r}'|^{-1})$.

With reference to Figure 9, and in view of Green's third identity applied to Ω_1^R and its boundary $\partial\Omega_1^R = \Gamma_1^R \cup S_1^R$ we obtain the bounded-domain integral representation

$$I_1[v_1; \Gamma_1^R](\mathbf{r}) - I_1[v_1; S_1^R](\mathbf{r}) = \begin{cases} v_1(\mathbf{r}), & \mathbf{r} \in \Omega_1^R, \\ 0, & \mathbf{r} \in \mathbb{R}^2 \setminus \Omega_1^R. \end{cases} \quad (50a)$$

Similarly, integrating over the domains Ω_2^R and Ω_3^R , whose boundaries are given by $\partial\Omega_2^R = \Gamma_2^R \cup \Gamma_{2,r}^R \cup \Gamma_1^R \cup \Gamma_{2,\ell}^R$ and $\partial\Omega_3^R = \Gamma_2^R \cup S_3^R$, respectively, the bounded-domain integral representations

$$I_2[v_2; \Gamma_2^R](\mathbf{r}) - I_2[v_2; \Gamma_1^R](\mathbf{r}) - I_2[v_2; \Gamma_{2,\ell}^R \cup \Gamma_{2,r}^R](\mathbf{r}) = \begin{cases} v_2(\mathbf{r}), & \mathbf{r} \in \Omega_2^R, \\ 0, & \mathbf{r} \in \mathbb{R}^2 \setminus \Omega_2^R, \end{cases} \quad (50b)$$

and

$$-I_3[v_3; \Gamma_2^R](\mathbf{r}) - I_3[v_3; S_3^R](\mathbf{r}) = \begin{cases} v_3(\mathbf{r}), & \mathbf{r} \in \Omega_3^R, \\ 0, & \mathbf{r} \in \mathbb{R}^2 \setminus \Omega_3^R \end{cases} \quad (50c)$$

result. In order to complete our calculations it suffices to evaluate the limiting values as $R \rightarrow \infty$ for the various integral quantities in (50) and for each one of the functions v_j in (39). Since, in view of equations (41), (42) and (43), these functions can be expressed as linear combinations of u_j^\uparrow , u_j^\downarrow , v_j^{gui} and v_j^{rad} in what follows we obtain the corresponding limiting values for each one of these functions. The desired representation formulae (51) as well as their N -layer versions (53) then follow directly from the limiting expressions thus found.

Case $j = 2$ for $v_2 = u_2^\uparrow$, $v_2 = u_2^\downarrow$, $v_2 = v_2^{\text{gui}}$ and $v_2 = v_2^{\text{rad}}$. In view of the decay of the integral kernels (49) and the fact that the total field v_2 remains bounded throughout Ω_2 (as it follows from equation (45)), we conclude that the term I_2 involving the integral over $\Gamma_{2,r}^R \cup \Gamma_{2,\ell}^R$ tends to zero as $R \rightarrow \infty$.

Case $j = 1, 3$ for $v_j = v_j^{\text{rad}}$. In order to estimate the terms I_j that involve integrals over the semi-circular curves S_1^R and S_3^R , in turn, we note that for $\mathbf{r}' \in S_j^R$ with $j = 1$ and $j = 3$ we have $|\mathbf{r}'| = R + O(1)$ and $\widehat{\mathbf{r}}' = (\cos \theta_j, \sin \theta_j) + O(R^{-1})$ as $R \rightarrow \infty$ —where the angles θ_j are as shown in Figure 9. Since v_j^{rad} in (43) for $j = 1, 3$ satisfies the Sommerfeld radiation condition (44), utilizing standard arguments [11] it can be shown that

$$I_j[v_j^{\text{rad}}; S_j^R] = o(1), \quad j = 1, 3, \quad \text{as } R \rightarrow \infty.$$

Case $j = 1, 3$ for $v_j = v_j^{\text{gui}}$. We now consider the quantity $I_1[v_1^{\text{gui}}; S_1^R]$, which, according to (45), is given by a linear combination of terms of the form $I_1[v_1^m; S_1^R]$ ($m = 1, \dots, M_j$), where $v_1^m(\mathbf{r}) = e^{-\gamma_1^m |y| + i\xi_1^m |x|}$ with $\gamma_1^m > 0$. From (49) and the fact that $v_1^m(\mathbf{r}') = e^{-\gamma_1^m R \sin \theta_1 + i\xi_1^m R |\cos \theta_1|}$ for $\mathbf{r}' = R(\cos \theta_1, \sin \theta_1) \in S_1^R$, $\theta_1 \in [0, \pi]$, we obtain

$$I_1[v_1^m; S_1^R](\mathbf{r}) \sim \sqrt{\frac{k_1 R}{8\pi}} e^{ik_1 R - i\frac{\pi}{4}} \times \int_0^\pi \left\{ \frac{i\gamma_1^m \sin \theta_1 + |\cos \theta_1| \xi_1^m}{k_1} - 1 \right\} e^{-ik_1 \mathbf{r} \cdot \widehat{\mathbf{r}}' - R(\gamma_1^m \sin \theta_1 - i\xi_1^m |\cos \theta_1|)} d\theta_1$$

as $R \rightarrow \infty$. Therefore

$$|I_1[v_1^m; S_1^R](\mathbf{r})| \leq \sqrt{\frac{k_1 R}{2\pi}} \left\{ 1 + \frac{|\gamma_1^m| + \xi_1^m}{k_1} \right\} \int_0^{\pi/2} e^{-\gamma_1^m R \sin \theta_1} d\theta_1.$$

The integral in the expression on the right-hand-side can be bounded utilizing the inequality $\sin \theta \geq 2\theta/\pi$, $\theta \in [0, \pi]$, and we thus conclude that $I_1[v_1^m; S_1^R] = O(R^{-1/2})$ as $R \rightarrow \infty$. Similarly, it can be shown that $I_3[v_3^m; S_3^R] = O(R^{-1/2})$, and consequently, in view of (45), we conclude that $I_j[v_j^{\text{gui}}; S_j^R] = O(R^{-1/3})$, $j = 1, 3$, as $R \rightarrow \infty$.

Case $j = 1$ for $v_1 = u_1^\uparrow$ and $v_1 = u_1^\downarrow$. We consider the term $I_1[u_1^\uparrow; S_1^R]$ first, where $u_1^\uparrow(\mathbf{r}) = e^{ik_{1x}x + ik_{1y}y}$, or, in polar coordinates, $u_1^\uparrow(\mathbf{r}') = e^{ik_1 R \cos(\theta_1 + \alpha)}$ for $\mathbf{r}' \in S_1^R$. Then, integration by parts yields

$$\begin{aligned} I_1[u_1^\uparrow; S_1^R](\mathbf{r}) &\sim \sqrt{\frac{k_1 R}{8\pi}} e^{ik_1 R - i\frac{\pi}{4}} \int_0^\pi \{\cos(\theta_1 + \alpha) - 1\} e^{-ik_1 \mathbf{r} \cdot \hat{\mathbf{r}}'} e^{ik_1 R \cos(\theta_1 + \alpha)} d\theta_1 \\ &= -\frac{e^{ik_1 R + i\frac{\pi}{4}}}{\sqrt{8\pi k_1 R}} \int_0^\pi \frac{\sin(\theta_1 + \alpha)}{1 + \cos(\theta_1 + \alpha)} e^{-ik_1 \mathbf{r} \cdot \hat{\mathbf{r}}'} \frac{d}{d\theta_1} e^{ik_1 R \cos(\theta_1 + \alpha)} d\theta_1 \\ &= -\frac{e^{ik_1 R + i\frac{\pi}{4}}}{\sqrt{8\pi k_1 R}} \left\{ \frac{\sin(\theta_1 + \alpha) e^{ik_1(-\mathbf{r} \cdot \hat{\mathbf{r}}' + R \cos(\theta_1 + \alpha))}}{1 + \cos(\theta_1 + \alpha)} \right\} \Big|_0^\pi - \\ &\quad \int_0^\pi e^{ik_1 R \cos(\theta_1 + \alpha)} \frac{d}{d\theta_1} \left(\frac{\sin(\theta_1 + \alpha) e^{-ik_1 \mathbf{r} \cdot \hat{\mathbf{r}}'}}{1 + \cos(\theta_1 + \alpha)} \right) d\theta_1 \Big\} = O(R^{-1/2}) \end{aligned}$$

as $R \rightarrow \infty$. In order to deal with the term $I_1[u_1^\downarrow; S_1^R]$ with $u_1^\downarrow(\mathbf{r}) = e^{ik_{1x}x - ik_{1y}y}$ we proceed similarly. Using the polar form $u_1^\downarrow(\mathbf{r}') = e^{ik_1 R \cos(\theta_1 - \alpha)}$ for $\mathbf{r}' \in S_1^R$ of the down-going wave we obtain

$$I_1[u_1^\downarrow; S_1^R](\mathbf{r}) \sim \sqrt{\frac{k_1 R}{8\pi}} e^{ik_1 R - i\frac{\pi}{4}} \int_0^\pi \{\cos(\theta_1 - \alpha) - 1\} e^{-ik_1 \mathbf{r} \cdot \hat{\mathbf{r}}'} e^{ik_1 R \cos(\theta_1 - \alpha)} d\theta_1.$$

Note that since $\alpha \in (-\pi, 0)$ we have $0 < \theta_1 - \alpha < 2\pi$. Thus, there is only one point of stationary phase within the domain of integration at $\theta_1 = \alpha + \pi$. A straightforward application of the method of stationary phase [2] then yields

$$I_1[u_1^\downarrow; S_1^R](\mathbf{r}) = -e^{ik_1(x \cos \alpha + y \sin \alpha)} + O(R^{-1/2}) = -u^{\text{inc}}(\mathbf{r}) + O(R^{-1/2}) \quad \text{as } R \rightarrow \infty.$$

(Notice that integrating by parts yields that the limit points of the integral give rise to contributions that decay as R^{-1} .)

Case $j = 3$ for $v_j = u_j^\downarrow$. This case concerns the term $I_3[u_3^\downarrow; S_3^R]$ with $u_3^\downarrow(\mathbf{r}') = e^{ik_{3x}x - ik_{3y}y}$, where $k_{3x} = k_1 \cos \alpha$ and $k_{3y} = \sqrt{k_3^2 - k_{3x}^2}$. We distinguish three possible cases, namely: (a) $k_3 < k_1 |\cos \alpha|$, (b) $k_3 = k_1 |\cos \alpha|$ ($k_3 = -k_1 \cos \alpha$ for $\alpha \in (-\pi, -\pi/2]$ or $k_3 = k_1 \cos \alpha$ for $\alpha \in (-\pi/2, 0)$), and (c) $k_3 > k_1 |\cos \alpha|$. Since in case (a) we have $k_{3y} = i\sqrt{k_1^2 \cos^2 \alpha - k_3^2}$, a calculation completely analogous to the one carried in the estimation of the term $I_1[u_1^m; S_1^R]$ shows that $I_3[u_3^\downarrow; S_3^R] = O(R^{-1/2})$. In case (b), in turn, we first consider $\alpha \in (-\pi/2, 0)$. Under this assumption $u_3^\downarrow(\mathbf{r}') = e^{ik_3 R \cos \theta_3}$ for $\mathbf{r}' \in S_3^R$, and consequently

$$I_3[u_3^\downarrow; S_3^R](\mathbf{r}) \sim \sqrt{\frac{k_3 R}{8\pi}} e^{ik_3 R - i\frac{\pi}{4}} \int_{-\pi}^0 \{\cos \theta_3 - 1\} e^{-ik_2(d_2 \sin \theta_3 + \mathbf{r} \cdot \hat{\mathbf{r}}') + iRk_3 \cos \theta_3} d\theta_3.$$

Splitting the integration domain and using the identity $\cos \theta - 1 = -\sin^2 \theta / (1 + \cos \theta)$ we obtain

$$\begin{aligned} I_3[u_3^\downarrow; S_3^R](\mathbf{r}) &\sim \sqrt{\frac{k_3 R}{8\pi}} e^{ik_3 R - i\frac{\pi}{4}} \left\{ -\int_{-\frac{\pi}{2}}^0 \frac{\sin^2 \theta_3}{1 + \cos \theta_3} e^{-ik_3(d_2 \sin \theta_3 - \mathbf{r} \cdot \hat{\mathbf{r}}') + iRk_3 \cos \theta_3} d\theta_3 + \right. \\ &\quad \left. \int_{-\pi}^{-\frac{\pi}{2}} \{\cos \theta_3 - 1\} e^{-ik_3(d_2 \sin \theta_3 + \mathbf{r} \cdot \hat{\mathbf{r}}') + iRk_3 \cos \theta_3} d\theta_3 \right\}. \end{aligned}$$

Integration by parts yields that the first integral above amounts to a quantity of order $O(R^{-1/2})$. The stationary point at $\theta = -\pi$ in the second integral, on the other hand, leads to

$$I_3 [u_3^\downarrow; S_3^R] (\mathbf{r}) = -\frac{e^{ik_3x}}{2} + O(R^{-1/2}).$$

Similarly, in the case $k_3 = -k_1 \cos \alpha$ for $\alpha \in (-\pi, \pi/2]$ it can be shown that $I_3 (u_3^\downarrow; S_3^R) = -e^{-ik_3x}/2 + O(R^{-1/2})$. In the case (c), finally, $u_3^\downarrow(\mathbf{r}') = a e^{ik_3 R \cos(\theta_3 - \alpha')}$, $\mathbf{r}' \in S_3^R$, where $a = e^{-ik_3 d_2 \sin \alpha'}$ and where the angle $\alpha' \in (-\pi, 0)$ is determined by the Snell's law $k_3 \cos \alpha' = k_1 \cos \alpha$. Thus, once again, integration by parts yields

$$\begin{aligned} I_3 [u_3^\downarrow; S_3^R] (\mathbf{r}) &\sim a \sqrt{\frac{k_3 R}{8\pi}} e^{ik_3 R - i\frac{\pi}{4}} \int_{-\pi}^0 \{\cos(\theta_3 - \alpha') - 1\} e^{-ik_3(d_2 \sin \theta_3 + \mathbf{r} \cdot \hat{\mathbf{r}}')} e^{ik_3 R \cos(\theta_3 - \alpha')} d\theta_3 \\ &= O(R^{-1/2}). \end{aligned}$$

Therefore, taking the limit as $R \rightarrow \infty$ in (50) we obtain

$$I_1 [v_1; \Gamma_1] (\mathbf{r}) + \delta u^{\text{inc}} (\mathbf{r}) = \begin{cases} v_1 (\mathbf{r}), & \mathbf{r} \in \Omega_1, \\ 0, & \mathbf{r} \in \mathbb{R}^2 \setminus \bar{\Omega}_1, \end{cases} \quad (51a)$$

$$I_2 [v_2; \Gamma_2] (\mathbf{r}) - I_2 [v_2; \Gamma_1] (\mathbf{r}) = \begin{cases} v_2 (\mathbf{r}), & \mathbf{r} \in \Omega_2, \\ 0, & \mathbf{r} \in \mathbb{R}^2 \setminus \bar{\Omega}_2, \end{cases} \quad (51b)$$

$$-I_3 [v_3; \Gamma_2] (\mathbf{r}) + \delta u_3^\parallel (\mathbf{r}) = \begin{cases} v_3 (\mathbf{r}), & \mathbf{r} \in \Omega_3, \\ 0, & \mathbf{r} \in \mathbb{R}^2 \setminus \bar{\Omega}_3, \end{cases} \quad (51c)$$

where u_3^\parallel in (51c) is given by

$$u_N^\parallel (\mathbf{r}) = \begin{cases} \frac{q_N e^{ik_1 x \cos \alpha}}{2} & \text{if } k_N = k_1 |\cos \alpha|, \\ 0 & \text{if } k_N \neq k_1 |\cos \alpha|, \end{cases} \quad (52)$$

with $N = 3$, and where $\delta = 0$ if $v_j = v_j^d$, and $\delta = 1$ if $v_j = \tilde{u}_j^p + v_j^d$ or $v_j = \tilde{u}_j^p$.

Remark A.1. *The total field representation (51) can easily be extended to problems of scattering by defects in the presence of layer media composed by $N > 3$ layers; the result is*

$$I_1 [v_1; \Gamma_1] (\mathbf{r}) + \delta u^{\text{inc}} (\mathbf{r}) = \begin{cases} v_1 (\mathbf{r}), & \mathbf{r} \in \Omega_1, \\ 0, & \mathbf{r} \in \mathbb{R}^2 \setminus \bar{\Omega}_1, \end{cases} \quad (53a)$$

$$I_j [v_j; \Gamma_j] (\mathbf{r}) - I_j [v_j; \Gamma_{j-1}] (\mathbf{r}) = \begin{cases} v_j (\mathbf{r}), & \mathbf{r} \in \Omega_j, \\ 0, & \mathbf{r} \in \mathbb{R}^2 \setminus \bar{\Omega}_j, \end{cases} \quad j = 2, \dots, N-1, \quad (53b)$$

$$-I_N [v_N; \Gamma_{N-1}] (\mathbf{r}) + \delta u_N^\parallel (\mathbf{r}) = \begin{cases} v_N (\mathbf{r}), & \mathbf{r} \in \Omega_N, \\ 0, & \mathbf{r} \in \mathbb{R}^2 \setminus \bar{\Omega}_N. \end{cases} \quad (53c)$$

References

- [1] M. I. Aksun, A. Alparslan, and K. A. Michalski. *Current status of closed-form Green's functions in layered media composed of natural and artificial materials*. 2009 International Conference on Electromagnetics in Advanced Applications, 2009.
- [2] N. Bleistein and R. A. Handelsman. *Asymptotic expansions of integrals*. Holt, Rinehart and Winston, 1975.
- [3] L. M. Brekhovskikh and O. Godin. *Acoustics of Layered Media II: Point Sources and Bounded Beams*, volume 10. Springer, 2013.
- [4] O. Bruno, M. Lyon, C. Pérez-Arancibia, and C. Turc. Windowed green function method for layered-media scattering. *SIAM Journal on Applied Mathematics*, 76(5):1871–1898, 2016.
- [5] O. P. Bruno and L. A. Kunyansky. A fast, high-order algorithm for the solution of surface scattering problems: Basic implementation, tests, and applications. *Journal of Computational Physics*, 169(1):80–110, 2001.
- [6] W. Cai. Algorithmic issues for electromagnetic scattering in layered media: Green's functions, current basis, and fast solver. *Advances in Computational Mathematics*, 16:157–174, 2002.
- [7] W. Cai and T. Yu. Fast Calculations of Dyadic Green's Functions for Electromagnetic Scattering in a Multilayered Medium. *Journal of Computational Physics*, 165:1–21, 2000.
- [8] W. C. Chew. *Waves and Fields in Inhomogeneous Media*, volume 522. IEEE Press, 1995.
- [9] M. H. Cho and W. Cai. A parallel fast algorithm for computing the Helmholtz integral operator in 3-D layered media. *Journal of Computational Physics*, 231(17):5910–5925, July 2012.
- [10] D. Colton and R. Kress. *Inverse Acoustic and Electromagnetic Scattering Theory*, volume 93. Springer, third edition, 2012.
- [11] D. L. Colton and R. Kress. *Integral Equation Methods in Scattering Theory*. Pure and Applied Mathematics. John Wiley & Sons Inc., first edition, 1983.
- [12] T. J. Cui and W. C. Chew. Efficient evaluation of Sommerfeld integrals for TM wave scattering by buried objects. *Journal of Electromagnetic Waves and Applications*, 12(5):607–657, 1998.
- [13] T. J. Cui and W. C. Chew. Fast evaluation of Sommerfeld integrals for EM scattering and radiation by three-dimensional buried objects. *IEEE Transactions on Geoscience and Remote Sensing*, 37(2):887–900, 1999.
- [14] J. A. DeSanto and P. A. Martin. On the derivation of boundary integral equations for scattering by an infinite one-dimensional rough surface. *The Journal of the Acoustical Society of America*, 102(1):67–77, July 1997.
- [15] J. A. DeSanto and P. A. Martin. On the derivation of boundary integral equations for scattering by an infinite two-dimensional rough surface. *Journal of Mathematical Physics*, 1998.
- [16] C. Jerez-Hanckes and J.-C. Nédélec. Asymptotics for Helmholtz and Maxwell Solutions in 3-D Open Waveguides. *Communications in Computational Physics*, 11(2):629–646, Feb. 2012.

- [17] N. N. Lebedev. *Special Functions and their Applications*. Prentice-Hall, 1965.
- [18] I. V. Lindell and E. Alanen. Exact Image Theory for the Sommerfeld Half-Space Problem, Part I: Vertical Magnetic Dipole. *IEEE Transactions on Antennas and Propagation*, 32(2):126–133, 1984.
- [19] K. A. Michalski and J. R. Mosig. Efficient computation of Sommerfeld integral tails—methods and algorithms. *Journal of Electromagnetic Waves and Applications*, 2016.
- [20] A. Nosich. Radiation conditions, limiting absorption principle, and general relations in open waveguide scattering. *Journal of Electromagnetic Waves and Applications*, 8(3):329–353, 1994.
- [21] M. O’Neil, L. Greengard, and A. Pataki. On the efficient representation of the half-space impedance Green’s function for the Helmholtz equation. *Wave Motion*, 51(1):1–13, 2014.
- [22] M. Paulus, P. Gay-Balmaz, and O. Martin. Accurate and efficient computation of the Green’s tensor for stratified media. *Physical Review E*, 62(4):5797, 2000.
- [23] C. Pérez-Arancibia and O. P. Bruno. High-order integral equation methods for problems of scattering by bumps and cavities on half-planes. *Journal of the Optical Society of America A*, 31(8):1738–1746, Aug. 2014.
- [24] C. A. Pérez Arancibia. *Windowed integral equation methods for problems of scattering by defects and obstacles in layered media*. PhD thesis, California Institute of Technology, 2017.
- [25] A. Sommerfeld. Über die Ausbreitung der Wellen in der drahtlosen Telegraphie. *Annalen der Physik*, 333(4):665–736, 1909.
- [26] G. G. Stokes. On the intensity of the light reflected from or transmitted through a pile of plates. In *Proceedings of the Royal Society of London*, 1860.